Modeling primaries of acoustic/elastic waves by one-return approximation

Ru-Shan Wu and Xiao-Bi Xie, University of California, Santa Cruz

The ability to model only primaries is very desirable in seismic exploration and can find broad applications in modeling, imaging, data processing, and interpretation. In this article, "primaries" mean the primary transmitted or reflected waves that involve only single interactions (transmission or reflection) at interfaces (sharp discontinuities) inside a heterogeneous medium. Primary-only modeling usually is much faster and more memory-efficient than full-wave methods, and, in addition, can provide "clean" seismograms free from multiples—a feature useful in testing certain features of migration/imaging or velocity analysis algorithms. This ability of modeling primary-only events also means the method can eliminate pure multiples from full-wave seismograms. The potential applications of primary-only modeling go beyond seismic modeling. For example, it can be applied as an extended one-way propagator to migration/imaging using unconventional waves (such as turning waves), reflected waves, or duplex waves for difficult targets.

Primary-only modeling methods emerged rather recently and still present many challenges. The method must calculate the primaries with the full-wave or near full-wave accuracy (not just their high-frequency asymptotic approximation). It needs to correctly handle all forward-scattering phenomena, including diffraction, refraction, focusing, multiple arrivals, and elastic-wave conversions. The accuracy of wide-angle scattering in elastic media with strong velocity contrasts remains an important issue. In this article, we summarize the development of the primary-only modeling method using the one-return approximation and elucidate its features and advantages through some numerical examples.

The local Born and the De Wolf approximations

The Born approximation is a weak scattering approximation, valid only when the scattered field is much smaller than the incident field. This implies that the heterogeneities are weak, and the propagation distance is short. However, the valid region of the Born approximation for forward scattering is very different from that for backscattering.

In the forward direction, scattered fields from different sections along the propagation path arrive at the calculation point in phase with the incident field such that they will be coherently superposed, leading to the linear increase of the total field. The Born approximation does not obey energy conservation, resulting in a catastrophic divergence for long-distance propagation.

Backscattering behaves quite differently. Since there is no incident wave in the backward direction, the total observed field is the sum of all backscattered fields from all scatterers. In addition, the size of coherent stacking for backscattered waves is about a quarter of a wavelength due to the two-way traveltime difference. Beyond this coherent region, their contributions will be cancelled out. For this reason, backscattering does not have catastrophic divergence in the Born approximation.

In the case where large phase change has accumulated, the Born approximation is no longer valid. The Rytov approximation holds as long as the scattering angle is sufficiently small. The Rytov approximation is based on the Rytov transform, which normalizes the total field u by the unperturbed field u_0 and expresses the perturbation of the field by a complex phase function ψ (i.e., $u/u_0 = e^{\psi}$). In the Born approximation, the scattered field is in the form of $u - u_0$. After a long propagation distance in heterogeneous media, the scattered field in the forward direction can be very large due to the accumulation of phase perturbations, rendering the Born approximation invalid. The complex phase function is a convenient and valid way to express the phase perturbation due to scattering in the forward direction. However, the approximation involved in the derivation of the Rytov approximation limited its use to small-angle scattering (Wu et al., 2007). In any case, the Rytov approximation is inappropriate for backscattering.

The De Wolf approximation is a multiple-forescattering/single-backscattering (MFSB) approximation, which has been introduced to overcome the limitation of the Born and Rytov approximations in long-range, forward propagation and primary backscattering calculations.

The De Wolf approximation splits the scattering potential into forescattering and backscattering parts, and renormalizes the incident field and Green's function into the forward renormalized field (incident field updating) and forward renormalized Green's function (Green's function updating). The forward renormalized field is the sum of an infinite subseries including all multiple-forescattered fields. The forward propagator (forward renormalized Green's function) is the sum of a similar subseries including multiple-forescattering renormalization. For backscattering, only the single backscattered field is calculated at each step and then propagated in the backward direction using the renormalized forward propagator (updated Green's function). The De Wolf approximation is also called the "one-return approximation" since there is only one point of return along the modeling path. It belongs to a type of distorted Born approximation. However, it uses the wave-theory-based, one-way propagator as the Green's function and distinguishes itself from the traditional ray-Born approximation in the category of distorted Born approximation.

Methodology of the one-return approximation modeling

Based on the above consideration, we can formulate the one-return simulation for modeling primary transmission and reflection. First, we consider the scalar-wave case and choose a main propagation direction. For example, we can use the

vertical direction for reflection modeling. We then slice the whole medium into thin slabs perpendicular to the propagation direction. Within each thin slab, the weak scattering condition holds. We apply the local Born approximation in each slab and obtain the total field

$$u = u_0 + G_l \varepsilon u_0 = u_0 + U \qquad (1)$$

where G_l is a Green's operator (propagator) for the thin slab, u_0 is the incident wave, ε is the scattering potential, and $U = G_l \varepsilon u_0$ is the scattered wave. If we split scattering potential into the forescattering and backscattering parts (i.e., $\varepsilon = \varepsilon_f + \varepsilon_b$), we have the transmitted wave at the exit of the thin slab as $G_l(1+\varepsilon_f)u_0$, and the backscattered wave at the entrance of the thin slab as $G_l \varepsilon_b u_0$. The flowchart in Figure 1a schematically illustrates this process.

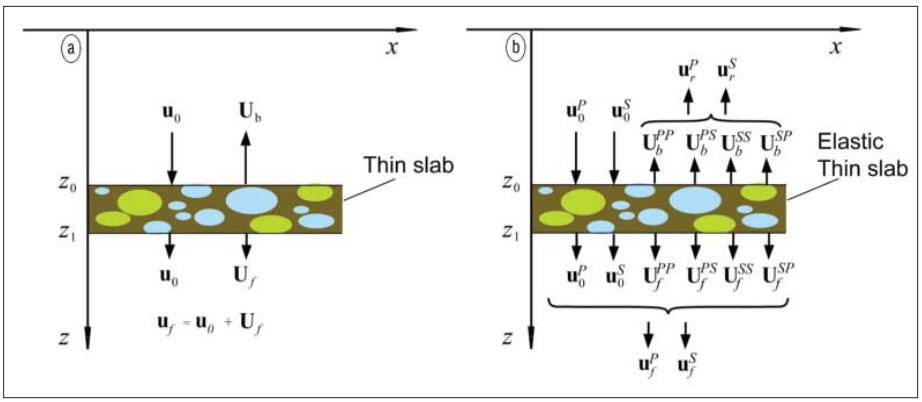

Figure 1. *Flowchart showing the interaction between the incident wave and a thin slab. (a) The scalar case where the scattering process generates a forescatted wave and a backscattered wave. The incident wave plus the forescattered wave form the transmitted wave as the updated incident wave for the next thin slab; the reflected wave is composed of backscattered waves. (b) In a general elastic case, different scattered waves are generated due to P- and S-wave scattering/conversion. Similar to the scalar case, the incident plus the forward-scattered waves form the transmitted wave, and the backscattered waves compose the reflections. Here the superscripts PP, PS, SS, and SP denote the P-to-P, P-to-S, S-to-S, and S-to-P scatterings.*

In a general heterogeneous elastic model, the situation is much more complex than for the scalar wave. Both incident and scattered waves can be P- and S-waves. An isotropic elastic model can be described with three material parameters, the density ρ and the Lamé constants λ and μ (or, equivalently, density ρ and P- and S-wave velocities α and β). For anisotropic models, more elastic parameters are involved. The interaction between incident waves with perturbations of different material parameters can generate different scattered waves with complex radiation patterns. Figure 1b schematically illustrates the interaction between the incident P- and S-waves with a thin slab. Here, at the entrance, u_0^P and u_0^S are incident waves and U_b^{PP}, U_b^{PS}, U_b^{SS}, and U_b^{SP} are different types of backscattered waves from different incident waves. Similar to the scalar-wave case, the incident and forward scattered waves combine into the transmitted waves (updated incident waves for the next thin slab). The backscattered waves form the reflections from the thin slab. Taking into consideration of complexities of elastic-waves (e.g., multicomponent, multiple material parameters, scattering patterns, and couplings between different wave modes), an equation system can be derived for calculating the elastic-wave scattering (Wu et al. 2007).

To obtain the wavefield in the entire model, we follow the De Wolf approximation and design an iterative scheme to calculate the wavefield. The flowchart shown in Figure 2 illustrates this process. The left side is for calculating the downgoing wave, and the right is for the upgoing wave. For the downgoing wave calculation, the $+z$ (downward) direction is chosen as the forward direction. Taking the ith slab as an example, the downgoing wave from the $(i\text{-}1)$th thin slab is the incident wave for the ith slab. After interacting with the slab, the forward (downgoing) wavefield $u_f^D(z_i)$ is generated at the exit and the backscattered (reflected) field $u_b(z_i)$ is

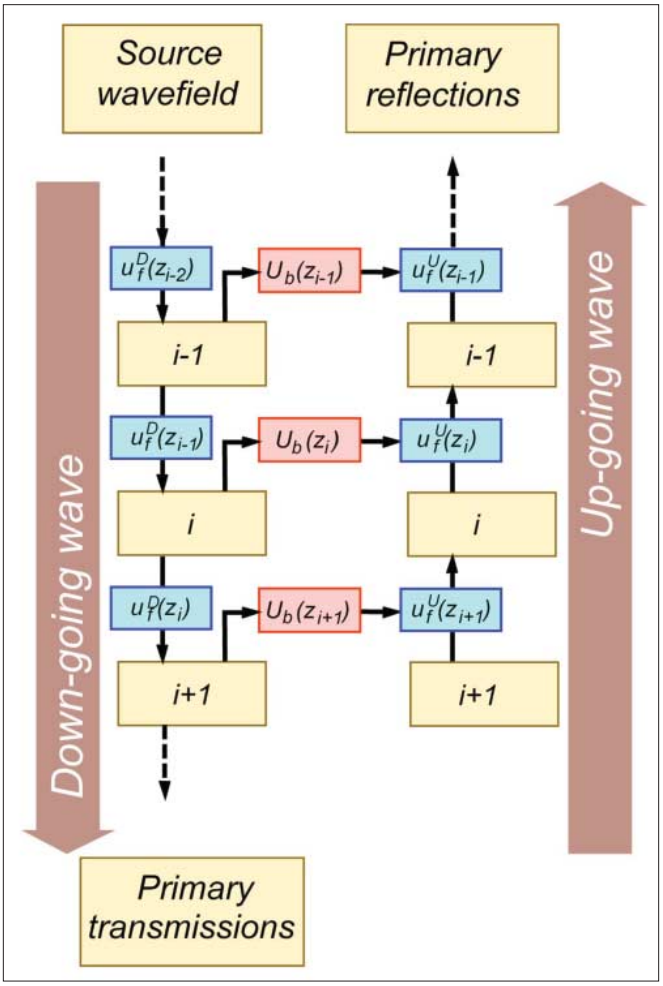

Figure 2. *Flowchart showing the calculation of primary reflections using the one-return approximation. u_f^D (left column) is the forescattering renormalized downgoing wave; u_f^U(right column) is the forescattering renormalized upgoing wave. In this survey setting (measurement on the surface), u_f^D is composed of purely a primary transmitted wave and while u_f^U includes all primary reflections: ($U_b(z_i)$, i=1....N). See text for details.*

generated at the entrance of the slab. The forward wavefield is used as the updated incident wave for the next slab while the reflected field is stored temporarily (shown in the central column). This iterative marching process forms the forward propagator (renormalized Green's function), which generates the primary transmitted waves. Next, as indicated on the right of Figure 2, we calculate the upgoing field by choosing $-z$ (upward) direction as the forward direction. At each level, we pick up the reflected (backscattered) fields, prestored at each level, and propagate them to the surface using the upgoing forward propagator. At the end of this process, we obtain the primary reflection from the entire model. All multiple forward scatterings in both downgoing and upgoing propagations are included; however, only single backscattering is involved for surface measurements.

To improve the accuracy of the forward propagator, we use the local Rytov approximation in place of the local Born approximation in dealing with the phase advance term to reduce the phase error accumulated during long-distance propagation. For large velocity perturbations and wide scattering angles, several approaches (e.g., hybrid implicit FD wide-angle correction or generalized screen series) can improve the wide-angle phase accuracy. Finally, we can formulate the method with a dual-domain technique by propagating the wavefield in the wavenumber domain with the reference velocity and interacting with the perturbations in the space domain. The entire procedure provides an efficient algorithm for calculating primary transmissions and reflections based on the De Wolf approximation.

Mathematically, the iterative process illustrated in Figure 2 is a sequential application of the thin-slab transmission operator, another way of expressing the De Wolf approximation for transmitted waves. The primary transmission is also equal to the downgoing Green's operator (forward propagator), $G_f^D = u_f^D$. The upgoing Green's operator can be formed similarly. Then the primary reflections on the surface can be calculated as the sum of single backscattered waves from all levels that are propagated to the surface by the renormalized upgoing Green's operator (forward propagator) G_f^U.

$$U_b^U(z_0) = \sum_{i=1}^{N} \left\{ G_l \left(1 + \varepsilon_f\right) \right\}^i U_b(z_i) = \sum_{i=1}^{N} G_f^U U_b(z_i) \quad (2)$$

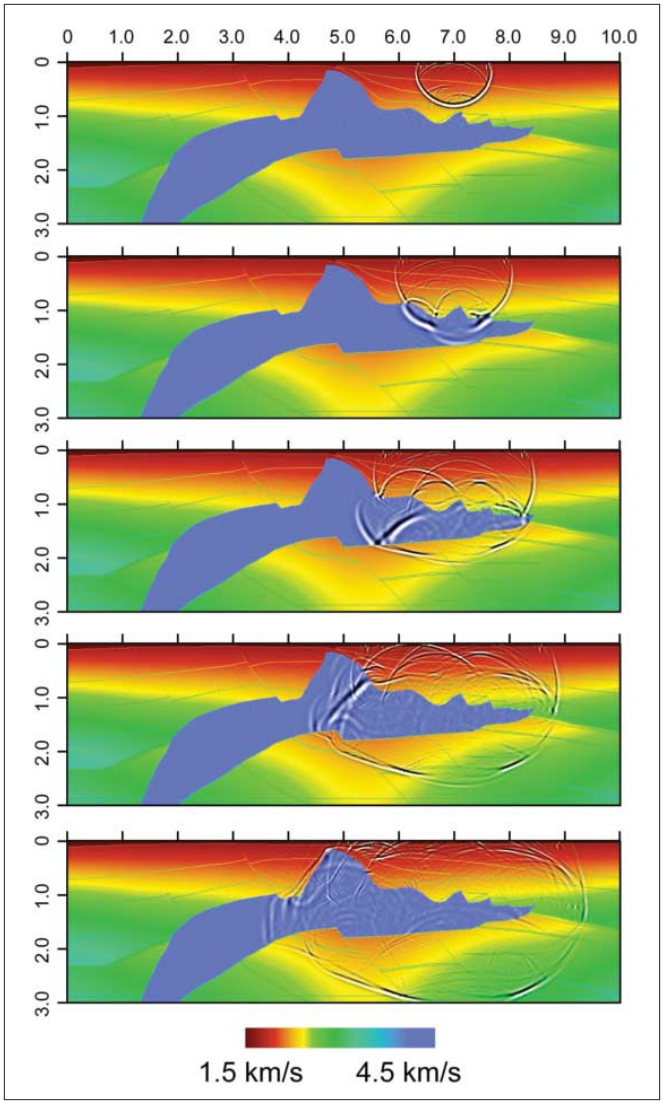

Figure 3. *Snapshots from the SEG/EAGE 2D acoustic salt model. The source is an 18-Hz Ricker wavelet. The snapshots are obtained by combining the upgoing and downgoing waves. Horizontal and vertical axes are distance (km).*

If we apply the one-return modeling (MFSB approximation) again to the upgoing waves, we can model secondarily backscattered waves. In a similar way, we can obtain higher-

	ϕ = 20%				ϕ = 23%				ϕ = 25%			
	α	β	ρ	σ	α	β	ρ	σ	α	β	ρ	σ
Shale	3170	1608	2.36	0.31	3170	1668	2.36	0.31	3170	1668	2.36	0.31
Gas	3500	2374	2.10	0.10	3350	2231	2.12	0.10	3188	2124	1.96	0.10
Oil	3734	2280	2.27	0.20	3527	2131	2.22	0.21	3362	2015	2.18	0.22
Brine	3749	2262	2.31	0.21	3551	2109	2.27	0.23	3399	1993	2.23	0.24

Table 1. *Reservoir model.*

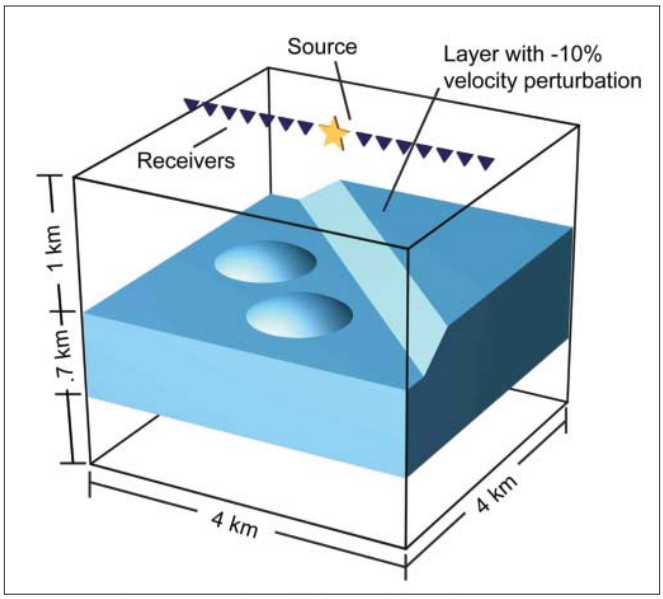

Figure 4. *The 3D French model for modeling elastic wave propagation. The shaded layer has a velocity perturbation of -10% for both P and S velocities.*

order backscattered waves using the De Wolf series.

Another remarkable feature of De Wolf modeling is the automatic formation of interface reflections. The heterogeneities in the medium can be either irregular, even random blobs, or large-scale blocked inclusions. If the thickness of the inclusion is much larger than the dominant wavelength, then the interface reflection will be automatically formed by the summation of a series of backscattered signals resembling the physical process. Only the waves from the first coherent zone contribute to the reflection. Scattered waves from other parts are all cancelled by each other due to destructive interference. It is also worth mentioning that the calculation with this formulation can preserve the finite frequency effect of reflections, while the theoretical reflection coefficients only predict the asymptotic values for infinite thick layers.

As an example, Figure 3 shows the primary waves calculated in the 2D acoustic SEG/EAGE salt model. These snapshots are composed from down- and upgoing waves. We see that the primary reflections from major sediment/salt boundaries and from the interfaces in the sedimentary layers are properly modeled.

3D reflection modeling of the elastic French model

As an example, we calculate primary reflections in a 3D elastic French model and compare the result with full-wave, finite-difference modeling. Figure 4 shows the model geometry. The parameters of the background medium are α = 3.6 *km/s*, β = 2.08 *km/s*, and ρ = 2.2 g/cm^3. The shaded layer has

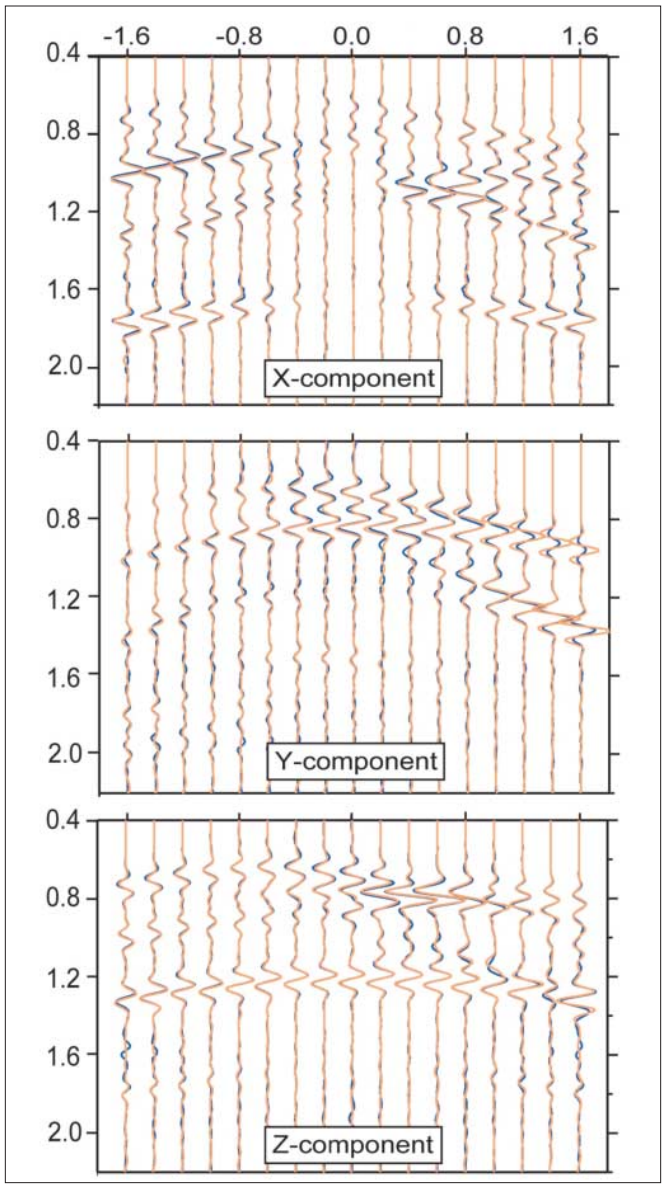

Figure 5. *Comparison between the synthetic seismograms calculated using the one-return method (blue lines) and the finite-difference method (red lines). From top to bottom are x-, y-, and z-components of displacement. Vertical axis is time (s) and horizontal axis is offset (km).*

	ϕ = 20				ϕ = 23%				ϕ = 25%			
	$\delta\alpha/\alpha$ (%)	$\delta\beta/\beta$ (%)	$\delta\rho/\rho$ (%)	δ	$\delta\alpha/\alpha$ (%)	$\delta\beta/\beta$ (%)	$\delta\rho/\rho$ (%)	δ	$\delta\alpha/\alpha$ (%)	$\delta\beta/\beta$ (%)	$\delta\rho/\rho$ (%)	δ
Gas	12.3	42.3	-11.0	0.10	5.7	33.7	-14.4	0.10	0.6	27.0	-17.0	0.10
Oil	17.8	36.7	-3.80		11.3	27.8	-5.9	0.21	6.1	20.8	-7.6	0.22
Brine	18.3	35.6	-2.10	0.21	12.0	26.4	-3.8	0.23	7.2	19.5	-5.5	0.24

Table 2. *Perturbation parameters for the reservoir model.*

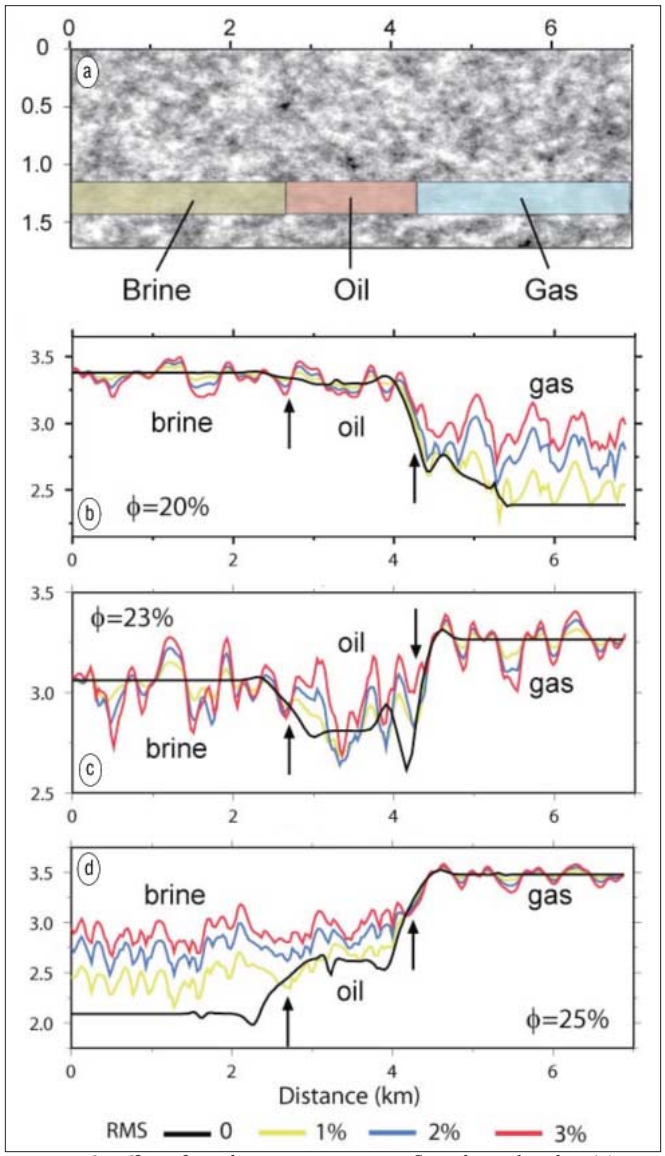

Figure 6. *Effect of random scattering on reflected amplitudes. (a) The sandstone model with random heterogeneities in the overburden and embedded reservoirs. Vertical and horizontal axes are distance (km). (b)–(d) Responses corresponding to porosities of 20%, 23%, and 25%, respectively. The vertical boundaries separating the gas, oil, and brine are indicated by arrows. Vertical axes are log amplitude, and horizontal axes are distance (km).*

a perturbation of -10% for both P- and S-wave velocities. The source and receiver locations are indicated. A Ricker wavelet with a dominant frequency of 10 Hz is used. Figure 5 compares three-component synthetic seismograms calculated using the one-return approximation (blue lines) and the finite-difference method (red lines). The y-component (anti-plane component) seismograms are very weak, and therefore are multiplied by a factor of 3 to show their details. We see that the results of the two methods are in excellent agreement for small-to-medium angle scatterings, particularly for the reflected and converted waves from the lower interface. With a similar accuracy, the one-return modeling is about 10 times faster than the finite-difference method.

Applications in reservoir reflection modeling with complex overburdens

To show the potential applications of this method, we use one-return modeling to examine the effect of random scattering in sedimentary rocks on AVO. Figure 6a shows a flat sandstone reservoir model bearing gas, oil, and brine. We calculate the actual reflectivities at the shale/gas, shale/oil, and shale/brine interfaces. The regions bearing the gas, oil ,and brine are between depths 1.2 and 1.5 km and are color-coded. To calculate the seismic response, reservoir parameters (Table 1) are used. To simulate the heterogeneous sedimentary rocks, a 2D random field is used to perturb the material parameters. The random field has an exponential correlation function with its horizontal and vertical correlation lengths of 100 and 40 m. The rms values used are 1%, 2%, and 3%. Both P- and S-wave velocities have the same rms perturbations, while the rms value for density is half of that used for velocities. Additional velocity, density, and Poisson ratio perturbations are added to the layer bearing gas, oil, and brine to simulate their properties and these parameters (Table 2). We consider a plane P-wave vertically incident on the reservoir.

To further examine the effect of porosity and rms fluctuations on the reflectivities, we calculate the maximum responses from different interfaces and for different material parameters. Figures 6b-d correspond to porosities of 20%, 23%, and 25%, respectively. The vertical axis is the logarithmic amplitude, and the locations of boundaries separating gas, oil, and brine are indicated by arrows. Black lines in these panels are results for models without overburden heterogeneities, in which the amplitudes fluctuations are caused by interferences from vertical boundaries separating different materials. The colored lines are for models with rms random velocity fluctuations of 1%, 2%, and 3%, respectively. Even for an overlying shale with heterogeneities as small as rms=1%, the piecewise

uniform reflection amplitudes are broken down due to the focusing and defocusing effect. The fluctuation of reflectivity is closely related to the statistical properties of heterogeneities and increases with the increase of the velocity fluctuations. The existence of a laterally varying overburden layer has strong effects on waves reflected from reservoir. It generates scattered waves and affects the reflection characteristics of local interfaces. For weak reflection sandstones, the scattering effect from heterogeneous overburden could be important and must be taken into account in AVO analysis.

Conclusions

Based on the De Wolf (multiple forescattering and single backscattering) approximation, the one-return method is an efficient technique for modeling primaries (primary transmitted and reflected waves) for acoustic and elastic models. With this method, all forward-scattering phenomena (including diffraction, refraction, focusing/defocusing, multipathing, and elastic-wave conversion) are built into the forward propagator (renormalized Green's function). However, only single backscattering is considered in calculating reflected waves. For the case of elastic waves, multiple material parameters, couplings between P- and S-wave modes, and scattering patterns are all considered in the algorithm. The method is very efficient and usually is an order of magnitude faster than the conventional full-wave simulation. It can be used for calculating primary transmission and reflection in a variety of applications such as modeling, imaging, and interpretation. With the capability of calculating the primary-only synthetic seismograms, it can be used to separate multiples from primaries. In seismic imaging, one-return modeling can be used for imaging difficult objects using waves from unconventional paths, such as reflected or duplex waves.

Suggested reading. "Wide-angle elastic wave one-way propagator in heterogeneous media and an elastic wave complex-screen method" by Wu (*Journal of Geophysical Research*, 1994). "A geometrical approach to the elastic complex screen" by Wild and Hudson (*Journal of Geophysical Research,* 1998). "Modeling elastic wave forward propagation and reflection using the complex-screen method" by Xie and Wu (*Journal of the Acoustical Society of America,* 2001). "One-way and one-return approximations (De Wolf approximation) for fast elastic wave modeling in complex media" by Wu et al. (in *Advances in Wave Propagation in Heterogeneous Earth*, Elsevier, 2007). Multiple forward scattering was also used in the surface-wave modeling: "Propagation of shear waves and surface waves in a laterally heterogeneous mantle by multiple forward scattering" by Friedrich (*Geophysical Journal International,* 1999). For the applications of one-return approximation in seismic imaging using unconventional waves: "One-return wave equation migration: Imaging of duplex waves" by Jin et al. (SEG 2006 *Expanded Abstracts*). "Cumulative forescattering single backscattering two-way wave equation migration" by Wang and Verm (SEG 2007 *Expanded Abstracts*). TLE

Corresponding author: wrs@pmc.ucsc.edu